*chemistry*

MDPI

*Article*

# Application of DFT/TD-DFT Frameworks in the Drug Delivery Mechanism: Investigation of Chelated Bisphosphonate with Transition Metal Cations in Bone Treatment

**Fatemeh Mollaamin [1,*] and Majid Monajjemi [2]**

[1] Department of Biomedical Engineering, Faculty of Engineering and Architecture, Kastamonu University, Kastamonu 37100, Turkey
[2] Department of Chemical Engineering, Central Tehran Branch, Islamic Azad University, Tehran 1496969191, Iran
* Correspondence: smollaamin@gmail.com

**Abstract:** Carbon nanotubes (CNTs) are applied in a drug delivery system, which can be reacted with different structures such biomolecules. Bones have vital functions and are the locations of biochemical reactions in cells that might be exposed various diseases. As different metal ions are integral components of bone tissue with different functions in the physiological cellular medium as well as in bone treatment, they can be used differently as a basis or as a supplement for various materials in the field of bone repair. Therefore, this research aims to represent the recent progress in conjugated bisphosphonate (BP)-divalent transition metal ions of $Mn^{2+}$, $Fe^{2+}$, and $Co^{2+}$ with an emphasis on the properties of interaction with a (6, 6) armchair carbon nanotube as a nanocarrier to exhibit the potential biomedical application of drug delivery. In this article, "CNT" linked to "BP" of alendronic acid, ibandronic acid, neridronic acid, and pamidronic acid, which are chelated to transition metal cations of $Mn^{2+}$, $Fe^{2+}$, and $Co^{2+}$, was investigated based on DFT insights for obtaining the electron charge density. Transition metals chelating with phosphonate groups, which are large with six O atoms with negative charges, are active in generating chelated complexes with the bisphosphonates [BPs- $Mn^{2+}$/$Fe^{2+}$/$Co^{2+}$] through the status of drug design. In this work, B3LYP/6-311+G(d,p)/lanl2dz we have estimated the susceptibility of CNT for conjugating alendronic acid, ibandronic acid, neridronic acid, and pamidronic acid, which are chelated to transition metal cations of $Mn^{2+}$, $Fe^{2+}$, and $Co^{2+}$ through NMR, NQR, IR, UV-VIS spectroscopy, and HOMO-LUMO analysis. Finally, the obtained results have confirmed that the possibility of applying CNT and BPs of alendronic acid, ibandronic acid, neridronic acid, and pamidronic acid becomes suitable in transition metal chelating for delivery application. The calculated HOMO–LUMO energy gaps for BPs of alendronic acid, ibandronic acid, neridronic acid, and pamidronic acid at the B3LYP/6-311+G (d,p) level have revealed that the energy gap reflects the chemical activity of the molecule.

**Keywords:** nanocarrier; BPs; alendronic acid; ibandronic acid; neridronic acid; pamidronic acid; transition metal ion



**Citation:** Mollaamin, F.; Monajjemi, M. Application of DFT/TD-DFT Frameworks in the Drug Delivery Mechanism: Investigation of Chelated Bisphosphonate with Transition Metal Cations in Bone Treatment. *Chemistry* **2023**, *5*, 365–380. https://doi.org/10.3390/chemistry5010027

Academic Editor: Maxim L. Kuznetsov

Received: 17 January 2023
Revised: 20 February 2023
Accepted: 22 February 2023
Published: 23 February 2023



## 1. Introduction

Bisphosphonates (BPs) are the principal group of drugs utilized to inhibit extensive disease in skeletal-related events. These structures coordinate with different transition metal ions and regulate homeostasis in the bone cells. Because of the intrinsic dynamic characteristics of ion–ligand conjugates of non-bonded transition metal, BPs adsorbed on the surface of nanocarriers of carbon atoms have harmonic mechanical properties with strong dynamic coordination, and the ability to detect the release of transition metal cations that consequently make them practical in different biomedical applications. BPs are primary medications for the cure of different bone disorders. The substituting a variety of side chains on the central carbon atom leads to the structural diversity of BPs. Due

to the pair of phosphate groups, BPs have the capacity to bind transition metal ions via coordination bonds, thereby forming self-assembled nanoparticles and nanostructures. In addition, many transition metal ions are involved in various biological activities in the human body [1–3].

Bone tissue tolerates constant rebuilding and achieves equilibrium by osteoblasts producing bone and osteoclasts destroying bone. The compounds of BPs prevent the digestion of bone by causing osteoclast cell death or apoptosis, which diminishes the speed of bone destruction [4].

The principal impact of the active BPs is to prevent bone resorption. In fact, these structures manifest as really strong inhibitors of resorption when tested in various conditions in vivo and in vitro. BP compounds stop bone resorption caused by different reasons in cells and organs. They prevent the formation of holes by isolated osteoclasts on mineral layers [5].

Generally, the physicochemical impacts of BPs are very close to those of pyrophosphate. Therefore, they prevent the formation, postpone the association, and decrease the dissolution of calcium phosphate compounds. All these impacts depend on the identified intention of these structures for solid-phase calcium phosphate, on the surface of which they attach strongly. This notable characteristic is the basis for the employment of these structures as skeletal markers in nuclear medicine and the foundation for their selective localization in bone when employed as drugs. Attention has been paid to enhancing the bioavailability and duration of action of a drug to modify therapeutic consequences. Drug delivery technique is able to change a drug's pharmacokinetics and specificity by formulating it with various ingredients, drug carriers, and medical equipment [6–10].

Nanomedicine covers a wide range of therapeutic applications, from nanoparticulate drug delivery systems including carbon nanotubes and layered double hydroxides, to in vitro (biosensor) and in vivo (imaging and implantable devices) diagnostics [11–16]. Nanomedicine in drug delivery is used to achieve the improved delivery of water insoluble drugs, delivery of large macromolecule drugs to intracellular sites of action, and codelivery of two or more drugs or therapeutic factors for combination therapy [17–19]. Since the exploration of CNTs in 1990s and the progress of their application in nanomedicine, these compounds are significant through their properties including rich electronic and thermal factors, great mechanical strength, high chemical stability, and extremely light weight [20–22]. These carriers indicate capability for transferring therapeutic factors such as proteins, DNA, antibodies, and drugs through the external wall or trapping them in cavity nanotubes as a capsule [23–27].

Nanotubes, with their intrinsic properties, have been considered potential candidates for drug delivery carriers. The capped ends of nanotubes may be opened up by oxidation, allowing for the insertion of molecules of interest inside the nanotube. Carbon nanotubes (CNTs) can easily penetrate cells, delivering drugs directly to the cytoplasm or nucleus.

CNTs are large molecules which are built by repeating a pattern of $sp^2$ hybridized carbon atoms in a hexagonal composition, rolled into a cylinder of approximately 2.5–100 nm in diameter. CNTs are long and tubular fullerene structures, which can be either single-walled (SWCNTs) or multiwalled (MWCNTs). SWCNTs are formed by rolling a single layer of graphite cylinder with a tube diameter of approximately 0.4–2 nm, while MWCNTs are multiple concentric cylindrical shells of graphite layers with length about 0.36 nm and diameter about 2–100 nm. Nanotubes conform to a perpendicular position with the cell membrane during uptake, perforating and diffusing through the lipid bilayer to enter the cytoplasm. Functionalized CNTs are easily internalized by cells through passive and endocytosis-independent mechanisms [28–33].

Bone cells in the human body are gradually and continually taken away and substituted with new ones by osteoblasts throughout life. The BPs act by reducing osteoclast activity and then reducing the overturn of bone or replacement of old bone cells. Once we start becoming old and, in particular, when we contract disease, bone is damaged or removed more quickly than our body can substitute it. This makes bones weakened, thin,

and much easier to break with even a small impact or a fall from standing height. Therefore, BP medications support us to maintain bone density and bone strength.

In fact, the most popular BP medications have a high amount of transition metal cations, among them $Ca^{2+}$, with which they can produce both soluble and insoluble compounds and aggregates, depending on the pH of the solution and the transition metal present. The BPs are separated into chemical branches based on the side chains of R1 and R2. A central carbon can be seen in BPs with two side chains of R1, R2, and two phosphate branches, which are bonded to $Ca^{2+}$ through O- of PO3 groups to maintain a high amount of $Ca^{2+}$ in human bone cells (Scheme 1) [34–40].

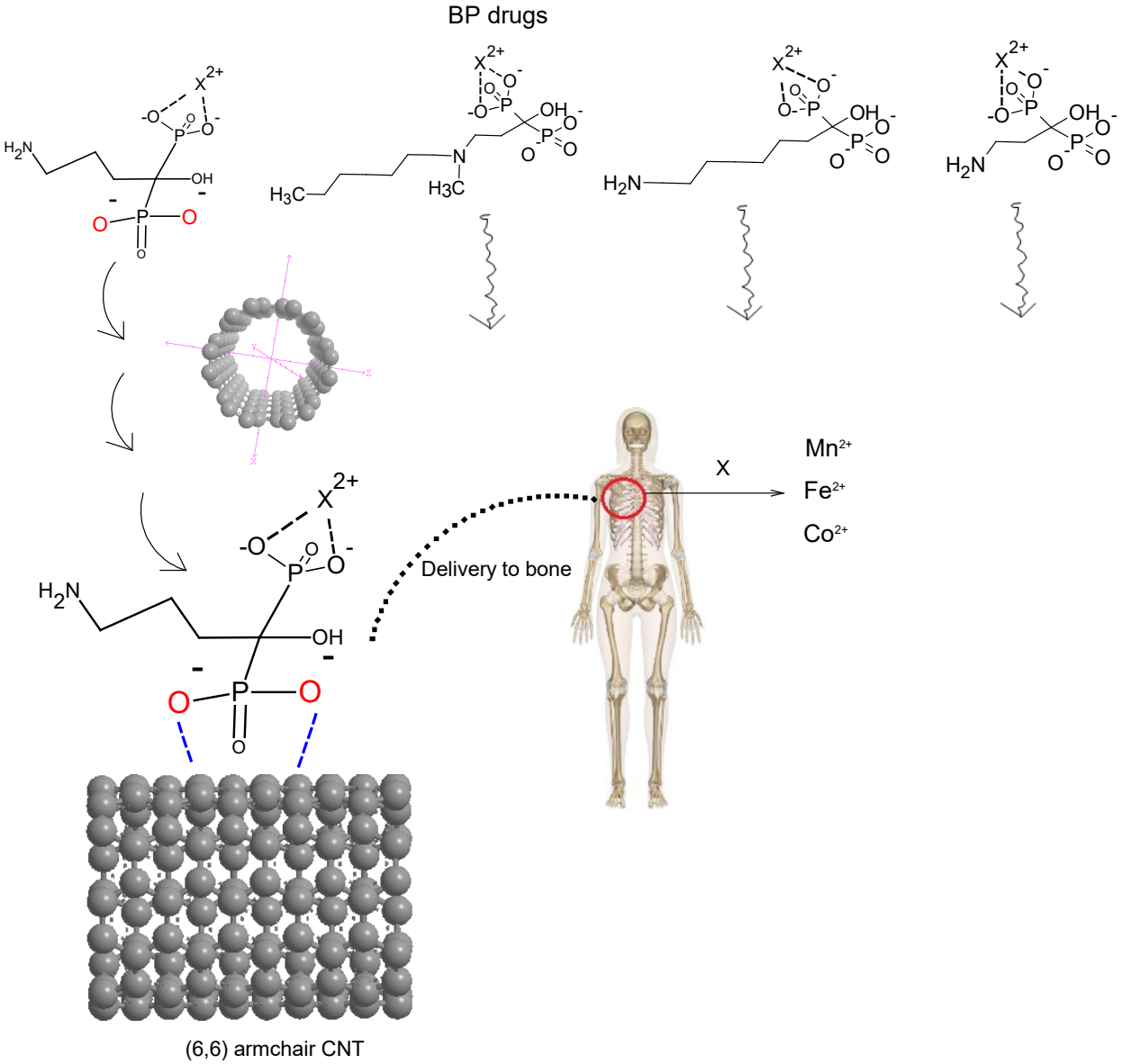


**Scheme 1.** Medication of BP-transition metal ion chelation of $Mn^{2+}$, $Fe^{2+}$, and $Co^{2+}$ through the $O^{-}$ of two $PO_3$ (phosphonate) groups covalently linked to carbon for six compounds of alendronic acid, ibandronic acid, neridronic acid, and pamidronic acid, and delivery to the bone tissue.

The metal ions are functionalized for different biochemical reactions, which are essential for the various steps of bone regeneration, because they affect the equilibrium between osteoblasts, osteoclasts, and osteocytes. Manganese is a vital element and is necessary for the appropriate function of a multitude of enzymes in living organisms. $Mn^{2+}$ also has a considerable impact on cell migration by modulating focal adhesion through integrins and

actin stress fiber formation, which makes Mn an appropriate selection for augmenting the growth and integration of bone-implantable materials [41].

Some researchers have reported a positive influence of iron oxide nanoparticles "IONPs" on the osteogenic differentiation of human "BMSCs" in vitro mediated by "MAPK" signaling. They illustrated that the negative effect of iron on osteogenesis resulting from enhanced reactive oxygen species "ROS" formation and ferritin activity can be prohibited by nanostructure compounds [42].

Based on previous studies, despite the negative impact of $Co^{2+}$ cations on osteogenic cells, hydroxyapatite (HAp) nanoparticles doped with $Co^{2+}$ indicated dose-dependent acceleration of osteogenesis, osteoporotic bone regeneration, and graft material replacement compared to HA-nanoparticles without $Co^{2+}$ [43].

In this article, we have focused more on recent BP drugs such as alendronic acid, ibandronic acid, neridronic acid, and pamidronic acid, which have been chelated with $Mn^{2+}$, $Fe^{2+}$, and $Co^{2+}$ conjugated on the surface of the (6, 6) armchair CNT, respectively (Scheme 1). This new generation of BPs of alendronic acid, ibandronic acid, neridronic acid, and pamidronic acid as the second and third generations of BP consists of nitrogen atoms in a side chain of R2 for promoting osteoclast apoptosis (Scheme 1). Therefore, patients obtain the cure with more intense nitrogen BPs rather than the earlier non-nitrogen BPs.

The conjugating of BPs of alendronic acid, ibandronic acid, neridronic acid, and pamidronic acid with $Mn^{2+}$, $Fe^{2+}$, and $Co^{2+}$ has been investigated in this study by forming relatively stable drugs for embedding on the (6, 6) armchair CNT as a drug delivery method (Scheme 2).

Thus, a series of quantum theoretical approaches has been accomplished for finding the optimized coordination of [BP- transition metal ion] chelation including O→$Mn^{2+}$, O→ $Fe^{2+}$, and O→ $Co^{2+}$ about 1.82Å with a DFT method of computations using the Gaussian 16 revision C.01 program (Scheme 2) [44].

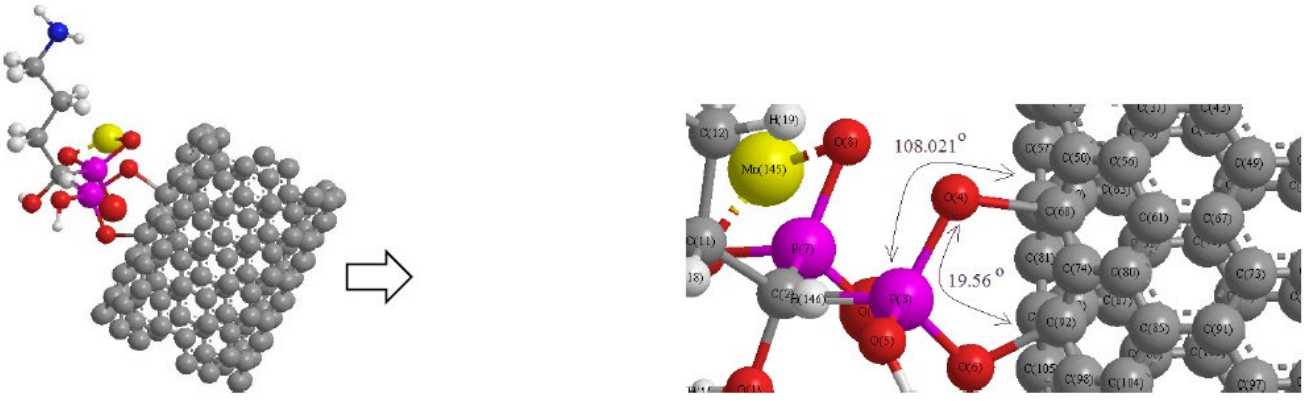


(**a**)

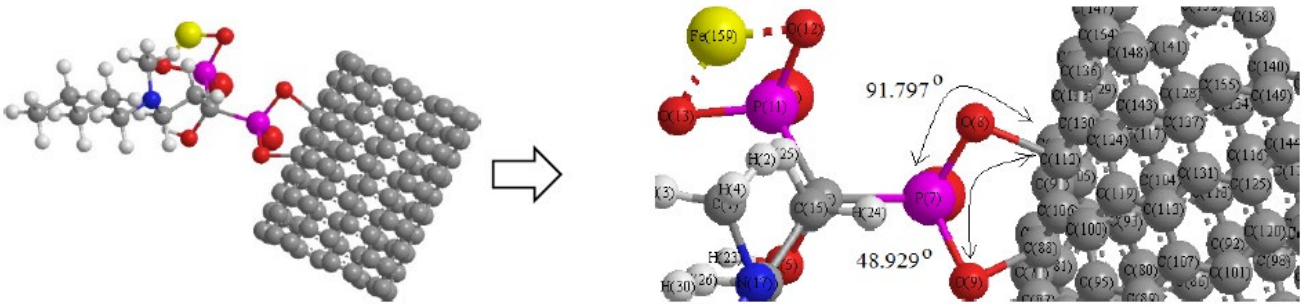


(**b**)

**Scheme 2.** *Cont.*

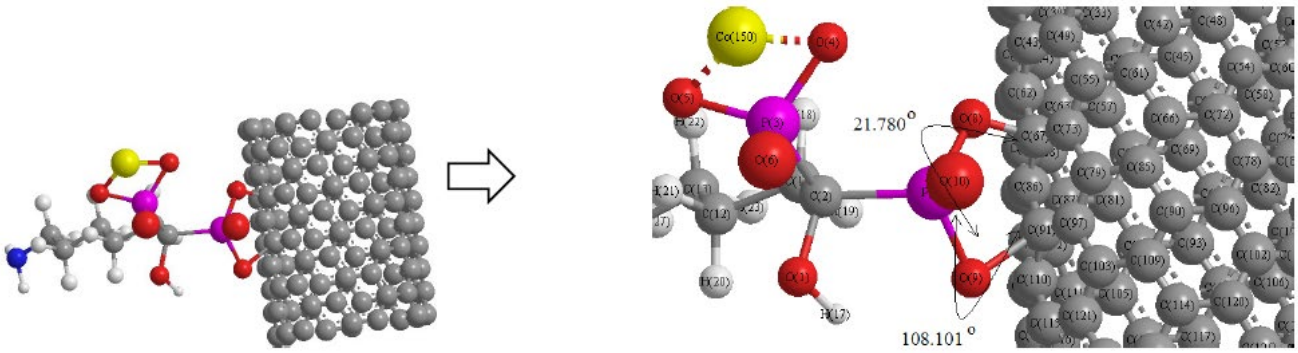


(**c**)

**Scheme 2.** Drug delivery of (**a**) alendronic acid, (**b**) ibandronic acid, and (**c**) neridronic acid conjugated with $Mn^{2+}$, $Fe^{2+}$, and $Co^{2+}$, respectively, adsorbed on the surface of (6, 6) armchair CNT.

## 2. Theoretical Foundation and Computational Methodology

In this study, the geometries were optimized at the framework of DFT using the three-parameter Becke's exchange [45,46] and Lee–Yang–Parr's correlation non-local function [47], usually known as the B3LYP method, and basis sets of lnl2dz for transition metal cations of $Mn^{2+}$, $Fe^{2+}$, and $Co^{2+}$, and 6-311+G(d,p) for other atoms including H, C, N, O, F, and P. Then, we described the electronic structure of the conjugated (6, 6) armchair CNT by BPs of alendronic acid, ibandronic acid, neridronic acid, and pamidronic acid chelated with $Mn^{2+}$, $Fe^{2+}$, and $Co^{2+}$ for measuring physico-chemical properties (Scheme 2).

In this investigation, the Onsager model was used, which was developed by Frisch, Wong and Wiberg, and utilizes spherical cavities. Even though this implies a less accurate description of the solute–solvent interface, this approximation simplifies the evaluation of energy formatives in geometry optimizations and frequency analysis [48].

Moreover, Cramer and Truhlar improved this model at the dipole level [49–53]. In fact, a cavity must have a physical sense such as the Onsager model, and a mathematical ability as often occurs in other descriptions of solvent impacts [54]. Specifically, the cavity has to keep out the solvent, and its frontiers must be the highest-probability part of the solute charge distribution [54,55].

Then, the gauge including atomic orbitals (GIAO) was adopted to solve the gauge problem in the calculation of nuclear magnetic shielding for the complexes of alendronic acid, ibandronic acid, neridronic acid, and pamidronic acid chelated with $Mn^{2+}$, $Fe^{2+}$, and $Co^{2+}$ conjugated onto the (6, 6) armchair SWCNT using density functional theory (DFT) calculations [56].

Chelation can be used between drugs and transition metal ions. For example, antibiotic drugs of the tetracycline and quinolone families are chelated with $Fe^{2+}$, $Ca^{2+}$, and $Mg^{2+}$ ions [57,58].

The chelation of BPs with cations in bone cells has been accomplished in this research by forming relatively stable complexes. Therefore, a group of quantum theoretical methods has been carried out for exploring the optimized structures of [BP-cations of $Mn^{2+}$, $Fe^{2+}$, $Co^{2+}$] cluster chelation conjugated onto the surface of the (6, 6) armchair SWCNT as the drug delivery method in human bone, with thermodynamic calculations and nuclear magnetic resonance analysis using the Gaussian 16 revision C.01 program [59].

## 3. Results and Discussion

In this work, we concentrated on the physical and chemical characteristics of BP–metal ion conjugates that have been embedded on the surface of the (6, 6) armchair CNT based on their linkage and stability. The intrinsic dynamic and energetic properties of the coordination bonds give these structures their special characteristics, which might be effective for drug delivery for the treatment of bone diseases.

The strength of the BP–metal ion–CNT depends on different factors such as the optimized geometry coordinates of interaction between BP and CNT, radius of transition metal ions, and other physico-chemical properties of BP compounds and CNT crystal.

The dynamic property of the BP–transition metal coordination bonds adsorbed on the surface of the (6, 6) armchair CNT exhibits electron transferring between the complex the and surface, which is related to the chelation bonding of the BPs of alendronic acid, ibandronic acid, neridronic acid, and pamidronic acid and transition metal ions of $Mn^{2+}$, $Fe^{2+}$, and $Co^{2+}$.

The embedded (6, 6) armchair CNT enables the facile encapsulation of BP medications of alendronic acid, ibandronic acid, neridronic acid, and pamidronic acid on its surface, and then the release of the encapsulated drug in the bone cell through a drug delivery approach.

The BP-based carbon nanotube stabilized by the dynamic BP–transition metal coordination has rich physiochemical characteristics consisting of thermodynamic properties of infrared (IR) spectrum, nuclear magnetic resonance (NMR), nuclear quadrupole resonance (NQR), electric potential, charge transfer, dipole moment, frontier of the highest occupied molecular orbital (HOMO) and the lowest unoccupied molecular orbital (LUMO), polarizability and hyperpolarizability, and UV-VIS properties during the adsorption mechanism.

### *3.1. NMR Analysis*

The BPs of alendronic acid, ibandronic acid, neridronic acid, and pamidronic acid have approximately shown identical behavior (30–590 ppm) for various atoms in the active sites of these compounds through the NMR properties (Figure 1). The sharpest NMR spectrum peak has been observed in almost 30 ppm for four BPs (alendronic acid, ibandronic acid, neridronic acid, and pamidronic acid). The weakest NMR spectrum peaks have appeared in approximately 200, 300, 400, and 600 ppm for all four BPs of alendronic acid, ibandronic acid, neridronic acid, and pamidronic acid (Figure 1).

The parameters of isotropic shielding tensor ($\sigma_{iso}$), anisotropic shielding tensor ($\sigma_{aniso}$), and eigenvalues of chemical shielding including $\sigma_{11}$, $\sigma_{22}$, and $\sigma_{33}$ resulted in NMR data for alendronic acid, ibandronic acid, neridronic acid, and pamidronic acid conjugated on the surface of the (6, 6) armchair CNT, respectively (Figure 2). The calculated results have indicated the SCF GIAO magnetic shielding tensor in ppm and charge transfer for oxygen (O), nitrogen (N), and phosphorus (P), exploring the active site of alendronic acid, ibandronic acid, neridronic acid, and pamidronic acid complexes of BPs as drugs for one disease's treatment. The computations have been run based on the B3LYP/6-311+G (d,p) level of theory using the Gaussian 16 revision C.01 program.

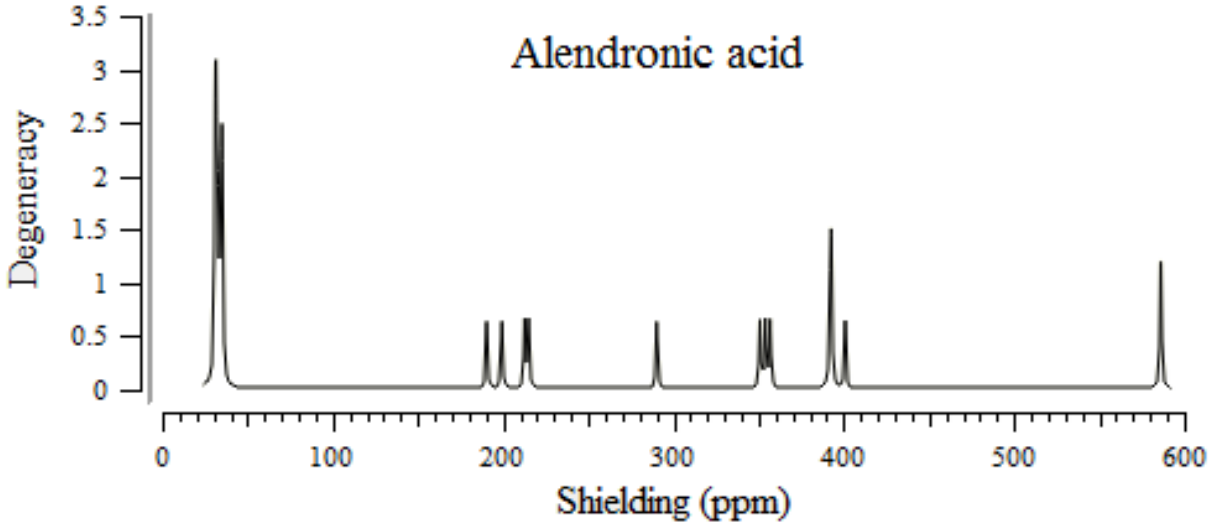


**Figure 1.** *Cont.*

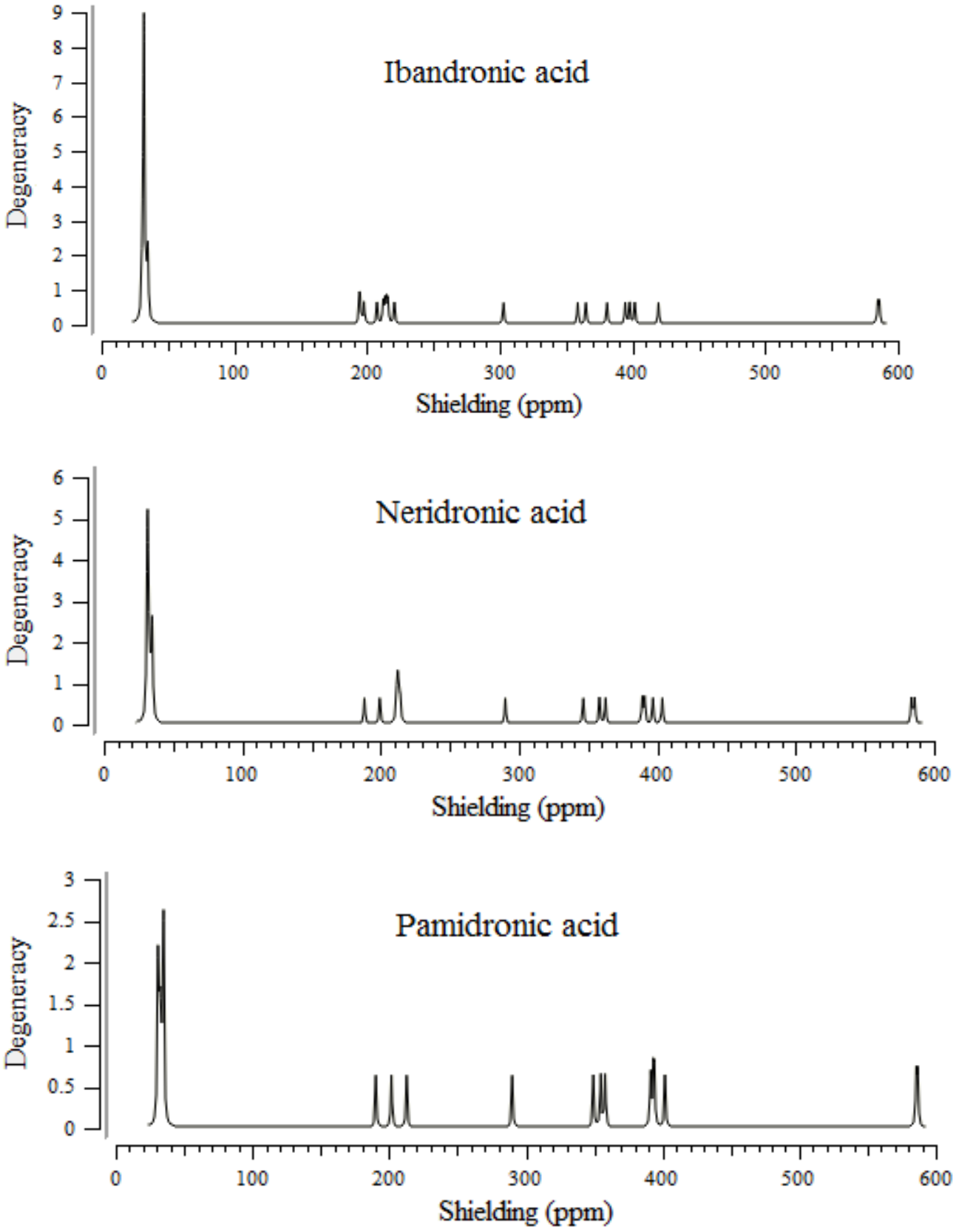


**Figure 1.** NMR spectra for alendronic acid, ibandronic acid, neridronic acid, and pamidronic acid in ppm conjugated on the surface of (6, 6) armchair CNT.

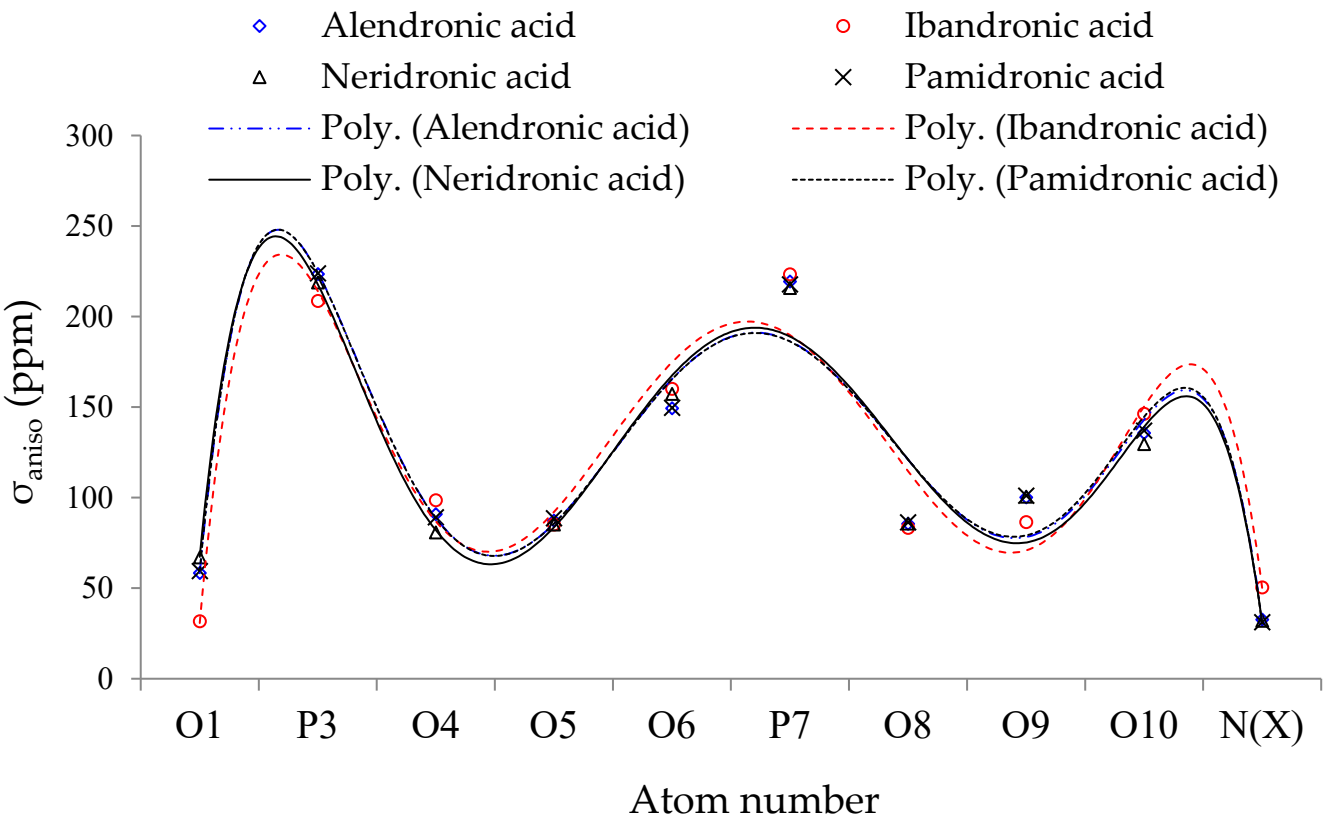


**Figure 2.** Calculated $\sigma_{aniso}$ of oxygen, nitrogen, and phosphorus atoms for alendronic acid, ibandronic acid, neridronic acid, and pamidronic acid in ppm conjugated on (6, 6) armchair using B3LYP/6-311+G(2d,p) level of theory.

Quantum chemical methods introduce the CS tensors in the principal axes system to evaluate the two parameters CSI (isotropic chemical-shielding) and CSA (anisotropic chemical-shielding) according to the equations [60]: CSI (ppm) = $(\sigma_{33}+ \sigma_{22} + \sigma_{11})/3$; CSA (ppm) = $\sigma_{33} - (\sigma_{22} + \sigma_{11})/2$.

Furthermore, the fluctuation in $\sigma_{aniso}$ versus atom number for BPs declares the maximum amounts for atoms of P3, P7, and O10 through alendronic acid, ibandronic acid, neridronic acid, and pamidronic acid, which represent the relation coefficients of $R^2_{alen}$ = 0.9141, $R^2_{iban}$ = 0.9253, $R^2_{neri}$ = 0.9202, and $R^2_{pami}$ = 0.9177, respectively.

### *3.2. NQR Method and Electric Potential*

A $^{14}$N-NQR approach has been accomplished for achieving the electric potential of carbon, nitrogen, oxygen, and phosphorus atoms for alendronic acid, ibandronic acid, neridronic acid, and pamidronic acid using the B3LYP/6-311+G (2d,p) level (Table 1).

There are two parameters that must be obtained from NQR experiments; the quadrupole coupling constant, $\chi$, and asymmetry parameter of the EFG tensor $\eta$: $\chi = e^2 Qq_{zz}/h$; $\eta = (q_{xx} - q_{yy})/q_{zz}$.

Table 1 shows the polynomial graphs (order = 3) of carbon, nitrogen, oxygen, and phosphorus atoms for alendronic acid, ibandronic acid, neridronic acid, and pamidronic acid with relation coefficients of $R^2_{alen}$ = 0.965, $R^2_{iban}$ = 0.8951, $R^2_{neri}$ = 0.9323, and $R^2_{pami}$ = 0.9657, respectively, due to the electric potential versus atomic charge, which have been achieved using the B3LYP/6-311+G (2d,p) method.

**Table 1.** Electric potential of some atoms resulting from $^{14}$N-NQR spectra for alendronic acid, ibandronic acid, neridronic acid, and pamidronic acid using B3LYP/6-311+G (d,p) level.

| Alendronic Acid | | Ibandronic Acid | | Neridronic Acid | | Pamidronic Acid | |
|---|---|---|---|---|---|---|---|
| **Atom** | **Electric Potential** | **Atom** | **Electric Potential** | **Atom** | **Electric Potential** | **Atom** | **Electric Potential** |
| C2 | −14.613324 | C2 | −14.611785 | C2 | −14.614456 | C2 | −14.610934 |
| O6 | −22.360828 | O6 | −22.34179 | O10 | −22.351188 | O10 | −22.354277 |
| O10 | −22.355359 | O10 | −22.340417 | O6 | −22.364336 | O6 | −22.361082 |
| O4 | −22.245017 | O5 | −22.247502 | O9 | −22.232377 | O9 | −22.235109 |
| O9 | −22.237996 | C18 | −14.736878 | O5 | −22.24993 | O5 | −22.247644 |
| O5 | −22.250791 | O8 | −22.220021 | O4 | −22.252005 | O4 | −22.242675 |
| O8 | −22.248466 | O9 | −22.24676 | C14 | −14.727871 | O8 | −22.246312 |
| N14 | −18.350535 | C16 | −14.72923 | O8 | −22.245526 | N13 | −18.342792 |
| O1 | −22.261584 | O4 | −22.245061 | N16 | −18.355079 | C12 | −14.686243 |
| C13 | −14.692506 | C14 | −14.701593 | 1O | −22.264629 | 1O | −22.262453 |
| C12 | −14.714985 | C12 | −14.686639 | C15 | −14.702393 | C11 | −14.699855 |
| C11 | −14.700335 | C19 | −14.706144 | C12 | −14.720226 | P7 | −53.958423 |
| P7 | −53.959567 | O1 | −22.265669 | C13 | −14.722867 | P3 | −53.957842 |
| P3 | −53.959198 | C17 | −14.729206 | C11 | −14.699184 | | |
| | | C15 | −14.729499 | P3 | −53.961477 | | |
| | | N13 | −18.333606 | P7 | −53.957784 | | |
| | | C11 | −14.699677 | | | | |
| | | P7 | −53.952902 | | | | |
| | | P3 | −53.960793 | | | | |

### *3.3. IR Spectra Analysis and Thermodynamic Properties*

The infrared (IR) technique for BPs conjugated on the surface of the (6, 6) armchair CNT has been accomplished using the B3LYP method and basis sets of lnl2dz for transition metal cations of $Mn^{2+}$, $Fe^{2+}$, and $Co^{2+}$, and 6-311+G(2d,p) for other atoms including H, C, N, O, and P to obtain the best amounts for geometrical coordination and thermochemical parameters. The greatest frequency fluctuation of IR spectra for alendronic acid, ibandronic acid, neridronic acid, and pamidronic acid can been seen between approximately 0 and 500 $cm^{-1}$, and 1000 and 1500 $cm^{-1}$, respectively (Figure 3).

Therefore, the physico-chemical properties of the relative harmonic frequencies, IR intensities, dipole moment, virial coefficient (−V/T), and ΔH, ΔG, and ΔS have determined the stability of BPs among [alendronic acid, ibandronic acid, neridronic acid, pamidronic acid -$Mn^{2+}$, $Fe^{2+}$, $Co^{2+}$] complexes conjugated on the surface of the (6, 6) armchair CNT as drugs for bone disorder treatment (Table 2). These nanostructures have proved the characteristics of the chelated bonding with transition metal cations of $Mn^{2+}$, $Fe^{2+}$, and $Co^{2+}$ using the drug delivery method (Table 2).

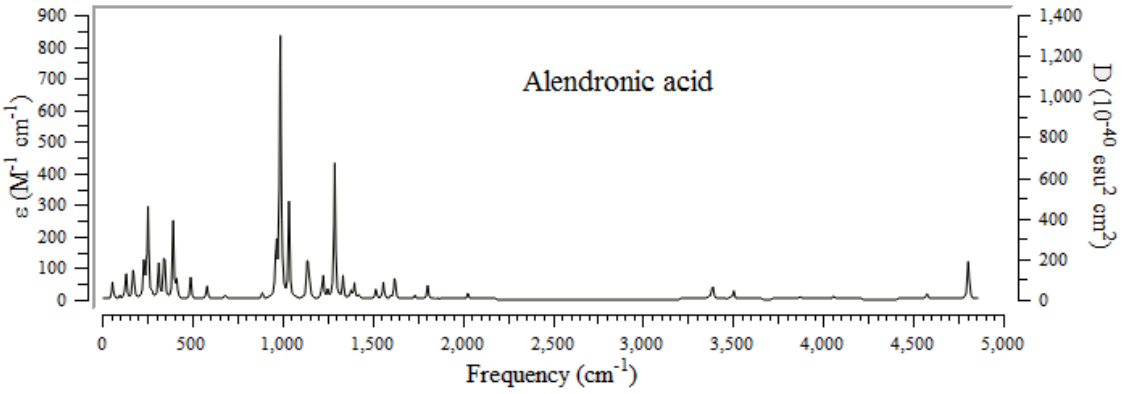


**Figure 3.** *Cont.*

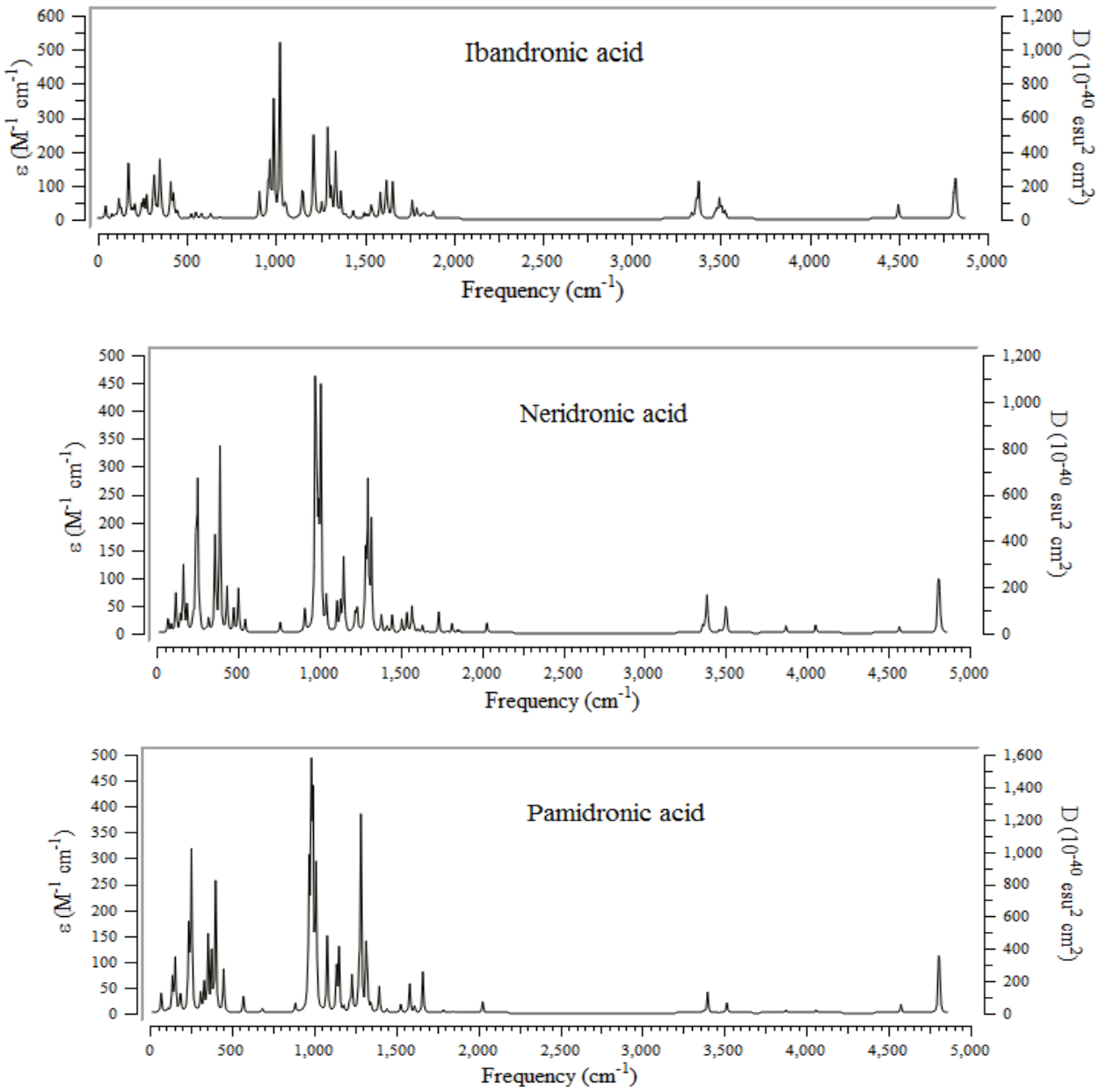


**Figure 3.** Computed IR spectra for alendronic acid, ibandronic acid, neridronic acid, and pamidronic acid of BPs conjugated onto (6, 6) armchair CNT using 6-311+G (2d,p) calculations.

**Table 2.** Calculated functions of harmonic frequencies ($cm^{-1}$); IR intensities (km/mol) in different normal modes; thermodynamic properties of ΔG and ΔH in kcal/mol, and ΔS in cal/mol.$K^{-1}$ at 300K; and optimized dipole moment (Debye).

| Compounds | ΔG × $10^{-3}$ (kcal/mol) | ΔH × $10^{-3}$ (kcal/mol) | ΔS (cal/K.mol) | Dipole Moment (Debye) | Virial Coefficient (−V/T) |
|---|---|---|---|---|---|
| **Alendronic acid-$Mn^{2+}$** | −879.232 | −879.200 | 108.813 | 3.3359 | 1.8754 |
| **Ibandronic acid-$Fe^{2+}$** | −1000.175 | −1000.137 | 128.466 | 2.9955 | 1.8643 |
| **Neridronic acid-$Co^{2+}$** | −927.610 | −927.575 | 118.208 | 4.4226 | 1.9722 |

These transition metal ions chelated to BPs medications help in the treatment of bone diseases such as fracture, osteoporosis, scoliosis, Paget's disease, rheumatoid arthritis, gout, bursitis, and other related disorders. The calculated properties explain the permeability and the solubility for the chosen BPs through biological membranes, which emerge as effective bioavailability indicators of the discovered BPs.

### *3.4. Frontier Molecular Orbital of HOMO and LUMO*

In this part, the ionization makes the highest occupied molecular orbital (HOMO) energy, and the electron affinity generates the lowest unoccupied molecular orbital (LUMO) energy, which have been measured and introduced for alendronic acid, ibandronic acid, neridronic acid, and pamidronic acid (Scheme 3). The HOMO, LUMO, and band energy gap (ev) represent the figurative description of the frontier molecular orbitals and their relative positive and negative districts, which are substantial operators for recognizing the molecular specifications of BPs.

As a matter of fact, the HOMO displays the susceptibility for giving an electron, while the LUMO, as an electron acceptor, depicts the ability to receive an electron. The energy gap ($\Delta E = E_{LUMO} - E_{HOMO}$) demonstrates the energy difference between the frontier HOMO and LUMO orbital, representing the resistance of the structure, and demonstrates the chemical activity of the compound. In this work, the energy gap shows how alendronic acid, ibandronic acid, neridronic acid, and pamidronic acid interact with the surface of the (6, 6) armchair CNT (Figure 4). In addition, the frontier molecular orbitals show an important function in the optical and electrical properties, like in UV-Vis spectra [61].

Figure 4 demonstrates the changes in energy gap ($E_{LUMO} - E_{HOMO}$) versus various effective compounds in BPs containing alendronic acid, ibandronic acid, neridronic acid, and pamidronic acid conjugated on the surface of the (6, 6) armchair CNT at the B3LYP/6-311+G(2d,p) level of theory.

### *3.5. UV-VIS Spectroscopy Analysis*

There is a critical factor as an energy gap between HOMO and LUMO for recognizing the characteristics of molecular electrical transport [62]. Based on the Frank–Condon principle, the maximum absorption peak (max) is related to a UV–visible spectrum of vertical excitation.

In this investigation, TD-DFT/6-311+G(2d,p) calculations have been carried out to identify the low-lying excited states of BPs. The results contain the vertical excitation energies, oscillator strength, and wavelength.

In the calculated value of the UV–visible spectrum of BPs, there is a maximum absorption band between 200 nm and 250 nm for alendronic acid, ibandronic acid, neridronic acid, and pamidronic acid. Strong adsorption has been observed for alendronic acid at about 225 nm; for ibandronic acid, 237.5 nm; for neridronic acid, 230 nm; and for pamidronic acid, 222 nm.

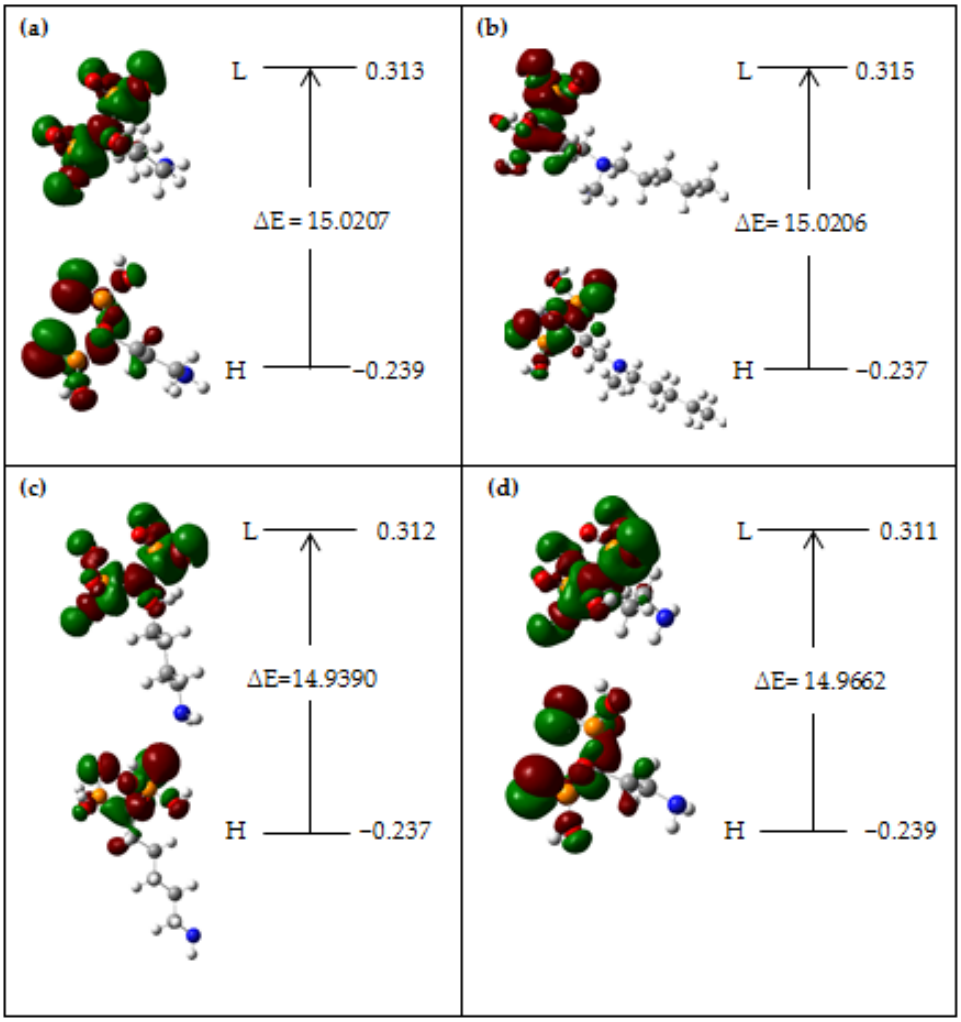


**Scheme 3.** Frontier orbitals of HOMO (a.u.), LUMO (a.u.), and band energy gap ($\Delta E = E_{LUMO} - E_{HOMO}$) (ev) for effective compounds of (**a**) alendronic acid, (**b**) ibandronic acid, (**c**) neridronic acid, and (**d**) pamidronic acid as the BP-targeted conjugates on the surface of (6, 6) armchair CNT.

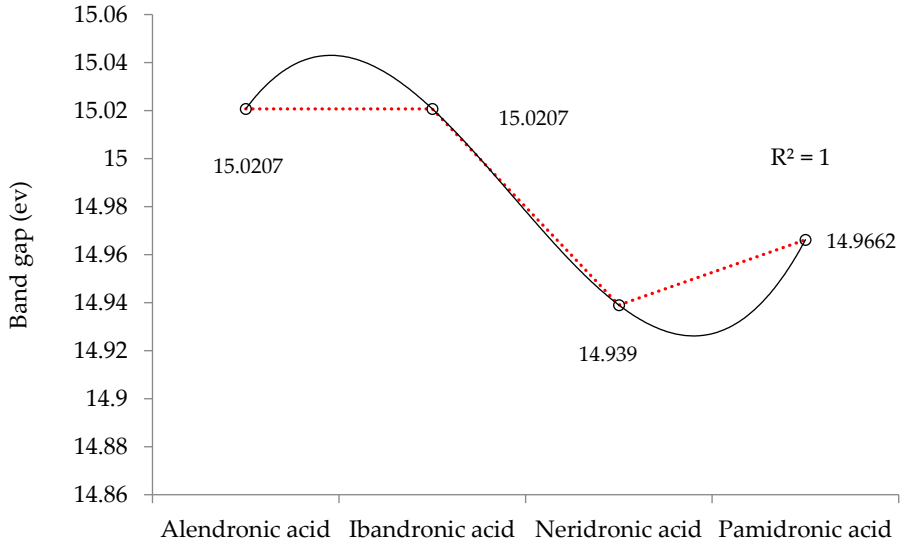


**Figure 4.** The band gap (ev) of HOMO-LUMO for BP-targeted alendronate, ibandronate, neridronate, and pamidronate.

## 4. Conclusions

The physico-chemical mode of action of various metal cations and their effect on bone tissue has indicated that their addition to present bone replacement materials can be the start of bone repair. Furthermore, metals can be captured with some drugs into carbon nanotubes, which support a continuous release to support the early induction of osteoblast differentiation. Drug delivery has the potential to ameliorate remedies for bone maladies. Some medication groups and nanostructures have illustrated potential, in particular, in terms of the delivery of drugs to bones, and enhanced the yield of treatment. Currently, bisphosphonates (BP) are being studied as targets for the delivery of conjugated medications to bone sites. BPs of alendronic acid, ibandronic acid, neridronic acid, and pamidronic acid have been considered for bone disease treatment due to the fact that they raise the osteoclast-mediated bone intake. In this research, through the incorporation of chelated cations of manganese, iron, cobalt, and nickel to BP drugs conjugated on the surface of the (6, 6) armchair CNT, the molecular geometry of the compounds in the ground state has been computed by using DFT/6-311+G(2d,p)/lanl2dz methods for obtaining several physical and chemical parameters.

Then, electronic, vibrational, and NMR measurements on complexes of [BPs-$Mn^{2+}$/$Fe^{2+}$/$Co^{2+}$] joined to a (6, 6) armchair carbon nanotube have been performed using B3LYP/6-311+G (2d,p)/lanl2dz. The HOMO-LUMO energy gap supported the analysis of the chemical reactivity of the molecule. TD-DFT calculations have indicated a strong effect for the most intense transition peak predicted in the case of the [BPs-$X^{2+}$] complexes. Third-order perturbation analyses of the NQR spectrum have been performed to investigate the effect of the metal transition cations' coordination on the different interactions within the studied molecules.

The outcomes of the above perceptions can support the recommendation of the various data gained for alendronic acid, ibandronic acid, neridronic acid, and pamidronic acid in the solvent, mainly because basis set functions are derived from a shift in the polarization of the ambience. It is notable that a growth in the dielectric constants raises the resistance and turnover of these BP medications for prohibiting the loss of bone density, osteoporosis cure, and other bone disorders. Finally, in this article, it has been observed that target-specific linkages between BPs and the chelated particles permit the liberation of drug upon bone binding. In fact, different drugs, nanostructures, and conjugation methodologies promise considerable scope for targeted drugs and the effective treatment of bone diseases.

**Author Contributions:** F.M.: Conceptualization and idea, methodology, software, validation, formal analysis, investigation, data curation, Writing—original draft preparation, visualization, supervision, project administration. M.M.: methodology, software, formal analysis, investigation, data curation, writing—review and editing, visualization, resources. All authors have read and agreed to the published version of the manuscript.

**Funding:** This research received no external funding.

**Institutional Review Board Statement:** Not applicable.

**Informed Consent Statement:** Not applicable.

**Data Availability Statement:** Not applicable.

**Acknowledgments:** In successfully completing this paper and its research, the authors are grateful to Kastamonu University for their support through the library, the laboratory, and scientific websites.

**Conflicts of Interest:** The authors declare no conflict of interest.

## References


1. Jang, H.L.; Jin, K.; Lee, J.; Kim, Y.; Nahm, S.H.; Hong, K.S.; Nam, K.T. Revisiting whitlockite, the second most abundant biomineral in bone: Nanocrystal synthesis in physiologically relevant conditions and biocompatibility evaluation. *ACS Nano* **2014**, *8*, 634–641. [CrossRef] [PubMed]
2. Mollaamin, F.; Özcan, S.S.; Özcan, E.; Monajjemi, M. Biomedical Applications of Bisphosphonate Chelating Agents by Metal Cations as Drug Design for Prevention and Treatment of Osteoporosis using QM/MM Method. *Biointerface Res. Appl. Chem.* **2023**, *13*, 329. [CrossRef]
3. Zaveri, T.D.; Lewis, J.S.; Dolgova, N.V.; Clare-Salzler, M.J.; Keselowsky, B.G. Integrin-directed modulation of macrophage responses to biomaterials. *Biomaterials* **2014**, *35*, 3504–3515. [CrossRef] [PubMed]
4. Kistler-Fischbacher, M.; Weeks, B.K.; Beck, B.R. The effect of exercise intensity on bone in postmenopausal women (part 2): A meta-analysis. *Bone* **2021**, *143*, 115697. [CrossRef] [PubMed]
5. Åkesson, K.E.; McGuigan, F.E.A. Closing the Osteoporosis Care Gap. *Curr. Osteoporos. Rep.* **2021**, *19*, 58–65. [CrossRef] [PubMed]
6. Tiwari, G.; Tiwari, R.; Sriwastawa, B.; Bhati, L.; Pandey, S.; Pandey, P.; Bannerjee, S.K. Drug delivery systems: An updated review. *Int. J. Pharm. Investig.* **2012**, *2*, 2–11. [CrossRef] [PubMed]
7. Li, J.; Zeng, M.; Shan, H.; Tong, C. Microneedle Patches as Drug and Vaccine Delivery Platform. *Curr. Med. Chem.* **2017**, *24*, 2413–2422. [CrossRef]
8. Bakhshi, K.; Mollaamin, F.; Monajjemi, M. Exchange and correlation effect of hydrogen chemisorption on nano V (100) surface: A DFT study by generalized gradient approximation (GGA). *J. Comput. Theor. Nanosci.* **2011**, *8*, 763–768. [CrossRef]
9. Ghalandari, B.; Monajjemi, M.; Mollaamin, F. Theoretical Investigation of Carbon Nanotube Binding to DNA in View of Drug Delivery. *J. Comput. Theor. Nanosci.* **2011**, *8*, 1212–1219. [CrossRef]
10. Singh, A.P.; Biswas, A.; Shukla, A.; Maiti, P. Targeted therapy in chronic diseases using nanomaterial-based drug delivery vehicles. *Signal Transduct. Target. Ther.* **2019**, *4*, 33. [CrossRef]
11. Mohsin, S.M.N.; Hussein, M.Z.; Sarijo, S.H.; Fakurazi, S.; Arulselvan, P.; Taufiq-Yap, Y.H. Characterisation and cytotoxicity assessment of UV absorbers-intercalated zinc/aluminium-layered double hydroxides on dermal fibroblast cells. *Sci. Adv. Mater.* **2014**, *6*, 648–658. [CrossRef]
12. Saifullah, B.; Hussein, M.Z.; Hussein-Al-Ali, S.H.; Arulselvan, P.; Fakurazi, S. Antituberculosis nanodelivery system with controlled-release properties based on para-amino salicylate-zinc aluminum-layered double-hydroxide nanocomposites. *Drug Des. Dev. Ther.* **2013**, *7*, 1365–1375. [CrossRef]
13. Barahuie, F.; Hussein, M.Z.; Hussein-Al-Ali, S.H.; Arulselvan, P.; Fakurazi, S.; Zainal, Z. Preparation and controlled-release studies of a protocatechuic acid-magnesium/aluminumlayered double hydroxide nanocomposite. *Int. J. Nanomed.* **2013**, *8*, 1975–1987. [CrossRef] [PubMed]
14. Kura, A.U.; Ali, S.H.H.A.; Hussein, M.Z.; Fakurazi, S.; Arulselvan, P. Development of a controlled-release anti-parkinsonian nanodelivery system using levodopa as the active agent. *Int. J. Nanomed.* **2013**, *8*, 1103–1110. [CrossRef] [PubMed]
15. Mohsin, M.S.M.N.; Hussein, Z.; Sarijo, S.H.; Fakurazi, S.; Arulselvan, P.; Taufiq-Yap, Y.H. Synthesis of (cinnamate-zinc layered hydroxide) intercalation compound for sunscreen application. *Chem. Cent. J.* **2013**, *7*, 26. [CrossRef]
16. Mohsin, S.M.N.; Hussein, M.Z.; Sarijo, S.H.; Fakurazi, S.; Arulselvan, P.; Taufiq-Yap, Y.H. Optimization of UV absorptivity of layered double hydroxide by intercalating organic UV-absorbent molecules. *J. Biomed. Nanotechnol.* **2014**, *10*, 1490–1500. [CrossRef] [PubMed]
17. Cao, X.; Deng, W.; Fu, M.; Zhu, Y.; Liu, H.; Wang, L.; Zeng, J.; Wei, Y.; Xu, X.; Yu, J. Seventy-two-hour release formulation of the poorly soluble drug silybin based on porous silica nanoparticles: In vitro release kinetics and in vitro/in vivo correlations in beagle dogs. *Eur. J. Pharm. Sci.* **2013**, *48*, 64–71. [CrossRef] [PubMed]
18. Ghaffarian, R.; Bhowmick, T.; Muro, S. Transport of nanocarriers across gastrointestinal epithelial cells by a new transcellular route induced by targeting ICAM-1. *J. Control. Release* **2012**, *163*, 25–33. [CrossRef] [PubMed]
19. Zhang, L.; Xue, H.; Cao, Z.; Keefe, A.; Wang, J.; Jiang, S. Multifunctional and degradable zwitterionic nanogels for targeted delivery, enhanced MR imaging, reduction-sensitive drug release, and renal clearance. *Biomaterials* **2011**, *32*, 4604–4608. [CrossRef]
20. Bethune, D.S.; Kiang, C.H.; de Vries, M.S.; Gorman, G.; Savoy, R.; Vazquez, J.; Beyers, R. Cobalt-catalysed growth of carbon nanotubes with single-atomic-layer walls. *Nature* **1993**, *363*, 605–607. [CrossRef]
21. Iijima, S.; Ichihashi, T. Single-shell carbon nanotubes of 1-nm diameter. *Nature* **1993**, *363*, 603–605. [CrossRef]
22. Dai, H. Carbon nanotubes: Opportunities and challenges. *Surf. Sci.* **2002**, *500*, 218–241. [CrossRef]
23. Abi, T.G.; Karmakar, T.; Taraphder, S. Proton affinity of polar amino acid sidechain analogues anchored to the outer wall of single walled carbon nanotubes. *Comput. Theor. Chem.* **2013**, *1010*, 53–66. [CrossRef]
24. Feng, W.; Ji, P. Enzymes immobilized on carbon nanotubes. *Biotechnol. Adv.* **2011**, *29*, 889–895. [CrossRef] [PubMed]
25. Chen, Q.; Kaneko, T.; Hatakeyama, R. Characterization of pulse-driven gas-liquid interfacial discharge plasmas and application to synthesis of gold nanoparticle-DNA encapsulated carbon nanotubes. *Curr. Appl. Phys.* **2011**, *11*, S63–S66. [CrossRef]
26. Mollaamin, F.; Monajjemi, M.; Salemi, S.; Baei, M.T. A Dielectric Effect on Normal Mode Analysis and Symmetry of BNNT Nanotube. *Fuller. Nanotub. Carbon Nanostruct.* **2011**, *19*, 182–196. [CrossRef]
27. Monajjemi, M.; Khaleghian, M.; Tadayonpour, N.; Mollaamin, F. The effect of different solvents and temperatures on stability of single-walled carbon nanotube: A QM/MD study. *Int. J. Nanosci.* **2010**, *09*, 517–529. [CrossRef]

28. Khalili Hadad, B.; Mollaamin, F.; Monajjemi, M. Biophysical chemistry of macrocycles for drug delivery: A theoretical study. *Russ. Chem. Bull.* **2011**, *60*, 238–241. [CrossRef]
29. Kofoed Andersen, C.; Khatri, S.; Hansen, J.; Slott, S.; Pavan Parvathaneni, R.; Mendes, A.C.; Chronakis, I.S.; Hung, S.-C.; Rajasekaran, N.; Ma, Z.; et al. Carbon Nanotubes—Potent Carriers for Targeted Drug Delivery in Rheumatoid Arthritis. *Pharmaceutics* **2021**, *13*, 453. [CrossRef]
30. Malik, D.K.; Baboota, S.; Ahuja, A.; Hasan, S.; Ali, J. Recent advances in protein and peptide drug delivery systems. *Curr Drug Deliv.* **2007**, *4*, 141–151. [CrossRef]
31. Cao, Z.; Kruczek, B.; Thibault, J. Monte Carlo Simulations for the Estimation of the Effective Permeability of Mixed-Matrix Membranes. *Membranes* **2022**, *12*, 1053. [CrossRef] [PubMed]
32. Katsumi, H.; Tanaka, Y.; Hitomi, K.; Liu, S.; Quan, Y.-S.; Kamiyama, F.; Sakane, T.; Yamamoto, A. Efficient Transdermal Delivery of Alendronate, a Nitrogen-Containing Bisphosphonate, Using Tip-Loaded Self-Dissolving Microneedle Arrays for the Treatment of Osteoporosis. *Pharmaceutics* **2017**, *9*, 29. [CrossRef] [PubMed]
33. Allen, T.M. Drug Delivery Systems: Entering the Mainstream. *Science* **2004**, *303*, 1818–1822. [CrossRef] [PubMed]
34. Mbese, Z.; Aderibigbe, B.A. Bisphosphonate-Based Conjugates and Derivatives as Potential Therapeutic Agents in Osteoporosis, Bone Cancer and Metastatic Bone Cancer. *Int. J. Mol. Sci.* **2021**, *22*, 6869. [CrossRef]
35. Rauner, M.; Taipaleenmäki, H.; Tsourdi, E.; Winter, E.M. Osteoporosis Treatment with Anti-Sclerostin Antibodies-Mechanisms of Action and Clinical Application. *J. Clin. Med.* **2021**, *10*, 787. [CrossRef] [PubMed]
36. Geiger, I.; Kammerlander, C.; Höfer, C.; Volland, R.; Trinemeier, J.; Henschelchen, M.; Friess, T.; FLS-CARE study group; Böcker, W.; Sundmacher, L. Implementation of an integrated care programme to avoid fragility fractures of the hip in older adults in 18 Bavarian hospitals—Study protocol for the cluster-randomised controlled fracture liaison service FLS-CARE. *BMC Geriatr.* **2021**, *21*, 43. [CrossRef]
37. Hayes, K.N.; He, N.; Brown, K.A.; Cheung, A.M.; Juurlink, D.N.; Cadarette, S.M. Over Half of Seniors Who Start Oral Bisphosphonate Therapy Are Exposed for 3 or More Years: Novel Rolling Window Approach and Patterns of Use. *Osteoporos. Int.* **2021**, *32*, 1413–1420. [CrossRef]
38. Sølling, A.S.; Christensen, D.H.; Darvalics, B.; Harsløf, T.; Thomsen, R.W.; Langdahl, B. Fracture Rates in Patients Discontinuing Alendronate Treatment in Real Life: A Population-Based Cohort Study. *Osteoporos. Int.* **2021**, *32*, 1103–1115. [CrossRef]
39. Kim, J.-W.; Yee, J.; Oh, S.-H.; Kim, S.-H.; Kim, S.-J.; Chung, J.-E.; Gwak, H.-S. Machine Learning Approaches for Predicting Bisphosphonate-Related Osteonecrosis in Women with Osteoporosis Using *VEGFA* Gene Polymorphisms. *J. Pers. Med.* **2021**, *11*, 541. [CrossRef]
40. Langdahl, B.L. Overview of treatment approaches to osteoporosis. *Br. J. Pharmacol.* **2021**, *178*, 1891–1906. [CrossRef]
41. Schramm, V.L. *Manganese in Metabolism and Enzyme Function*; Elsevier: Amsterdam, The Netherlands, 2012.
42. Wang, Q.; Chen, B.; Cao, M.; Sun, J.; Wu, H.; Zhao, P.; Xing, J.; Yang, Y.; Zhang, X.; Ji, M.; et al. Response of MAPK pathway to iron oxide nanoparticles in vitro treatment promotes osteogenic differentiation of hBMSCs. *Biomaterials* **2016**, *86*, 11–20. [CrossRef] [PubMed]
43. Ignjatović, N.; Ajduković, Z.; Savić, V.; Najman, S.; Mihailović, D.; Vasiljević, P.; Stojanović, Z.; Uskoković, V.; Uskoković, D. Nanoparticles of cobalt-substituted hydroxyapatite in regeneration of mandibular osteoporotic bones. *J. Mater. Sci. Mater. Med.* **2013**, *24*, 343–354. [CrossRef] [PubMed]
44. Frisch, M.J.; Trucks, G.W.; Schlegel, H.B.; Scuseria, G.E.; Robb, M.A.; Cheeseman, J.R.; Scalmani, G.; Barone, V.; Mennucci, B.; Petersson, G.A.; et al. *Gaussian 16, Revision C.01*; Gaussian, Inc.: Wallingford, CT, USA, 2016.
45. Koch, W.; Holthausen, M.C. *A Chemist's Guide to Density Functional Theory*, 2nd ed.; Wiley-VCH: Weinheim, Germany, 2002.
46. Becke, A.D. Density-functional thermochemistry. III. The role of exact exchange. *J. Chem. Phys.* **1993**, *98*, 5648–5652. [CrossRef]
47. Lee, C.; Yang, W.; Parr, R.G. Development of the Colle-Salvetti correlation-energy formula into a functional of the electron density. *Phys. Rev. B* **1988**, *37*, 785–789. [CrossRef]
48. Tahan, A.; Mollaamin, F.; Monajjemi, M. Thermochemistry and NBO analysis of peptide bond: Investigation of basis sets and binding energy. *Russ. J. Phys. Chem. A* **2009**, *83*, 587–597. [CrossRef]
49. Cramer, C.J.; Truhlar, D.G. PM3-SM3: A general parameterization for including aqueous solvation effects in the PM3 molecular orbital model. *J. Comp. Chem.* **1992**, *13*, 1089–1097. [CrossRef]
50. Zhou, J.; Doi, M. Derivation of Two-Fluid Model Based on Onsager Principle. *Entropy* **2022**, *24*, 716. [CrossRef]
51. Chambers, C.C.; Hawkins, G.D.; Cramer, C.J.; Truhlar, D.G. Model for aqueous solvation based on class IV atomic charges and first solvation shell effects. *J. Phys. Chem.* **1996**, *100*, 16385–16398. [CrossRef]
52. Sher, E.; Moshkovich-Makarenko, I.; Moshkovich, Y.; Cukurel, B. Implementation of the Onsager Theorem to Evaluate the Speed of the Deflagration Wave. *Entropy* **2020**, *22*, 1011. [CrossRef]
53. Onsager, L.J. Electric Moments of Molecules in Liquids. *J. Am. Chem. Soc.* **1936**, *58*, 1486–1493. [CrossRef]
54. Tomasi, J. Cavity and reaction field: "robust" concepts. Perspective on "Electric moments of molecules in liquids". *Theor. Chem. Acc.* **2000**, *103*, 196–199. [CrossRef]
55. Mollaamin, F.; Ilkhani, A.; Sakhaei, N.; Bonsakhteh, B.; Faridchehr, A.; Tohidi, S.; Monajjemi, M.; Fatemeh, M.; Alireza, I.; Neda, S.; et al. Thermodynamic and solvent effect on dynamic structures of nano bilayer-cell membrane: Hydrogen bonding study. *J. Comput. Theor. Nanosci.* **2015**, *12*, 3148–3154. [CrossRef]

56. Monajjemi, M.; Baie, M.T.; Mollaamin, F. Interaction between threonine and cadmium cation in [Cd(Thr)] (n = 1-3) complexes: Density functional calculations. *Russ. Chem. Bull.* **2010**, *59*, 886–889. [CrossRef]
57. Tanaka, S.; Tanaka, Y. RANKL as a therapeutic target of rheumatoid arthritis. *J. Bone Miner. Metab.* **2021**, *39*, 106–112. [CrossRef] [PubMed]
58. Vassaki, M.; Kotoula, C.; Turhanen, P.; Choquesillo-Lazarte, D.; Demadis, K.D. Calcium and Strontium Coordination Polymers as Controlled Delivery Systems of the Anti-Osteoporosis Drug Risedronate and the Augmenting Effect of Solubilizers. *Appl. Sci.* **2021**, *11*, 11383. [CrossRef]
59. Rauch, L.; Hein, R.; Biedermann, T.; Eyerich, K.; Lauffer, F. Bisphosphonates for the Treatment of Calcinosis Cutis-A Retrospective Single-Center Study. *Biomedicines* **2021**, *9*, 1698. [CrossRef]
60. Fry, R.A.; Kwon, K.D.; Komarneni, S.; Kubicki, J.D.; Mueller, K.T. Solid-State NMR and Computational Chemistry Study of Mononucleotides Adsorbed to Alumina. *Langmuir* **2006**, *22*, 9281–9286. [CrossRef]
61. Aihara, J. Reduced HOMO−LUMO Gap as an Index of Kinetic Stability for Polycyclic Aromatic Hydrocarbons. *J. Phys. Chem. A* **1999**, *103*, 7487–7495. [CrossRef]
62. Silverstein, R.M.; Bassler, G.C.; Morrill, T.C. *Spectrometric Identification of Organic Compounds*, 5th ed.; John Wiley & Sons, Inc.: New York, NY, USA, 1981.